A Universal Double-Side Passivation for High Open-Circuit Voltage in Perovskite Solar Cells: Role of Carbonyl Groups in Poly(methyl methacrylate)

Jun Peng, Jafar I. Khan, Wenzhu Liu, Esma Ugur, The Duong, Yiliang Wu, Heping Shen, Kai Wang, Hoang Dang, Erkan Aydin, Xinbo Yang, Yimao Wan, Klaus J. Weber, Kylie R. Catchpole, Frédéric Laquai, Stefaan De Wolf, Thomas P. White**

Jun Peng, Dr. The Duong, Yiliang Wu, Dr. Heping Shen, Dr. Yimao Wan, A/Prof. Klaus J. Weber, Prof. Kylie R. Catchpole and A/Prof. Thomas P. White
Research School of Engineering, The Australian National University, Canberra, ACT 2601, Australia
E-mail: thomas.white@anu.edu.au

Dr. Jafar I. Khan, Dr. Wenzhu Liu, Esam Ugur, Dr. Kai Wang, Dr. Hoang Dang, Dr. Erkan Aydin, Dr. Xinbo Yang, A/Prof. Frédéric Laquai and A/Prof. Stefaan De Wolf
King Abdullah University of Science and Technology (KAUST), KAUST Solar Center (KSC), Physical Sciences and Engineering Division (PSE), Thuwal 23955-6900, Kingdom of Saudi Arabia
E-mail: stefaan.dewolf@kaust.edu.sa

Keywords: non-radiative recombination, under-coordinated Pb atoms, passivation, carbonyl group, perovskite solar cells

Abstract

The performance of state-of-the-art perovskite solar cells is currently limited by defect-induced recombination at interfaces between the perovskite and the electron and hole transport layers. These defects, most likely under-coordinated Pb and halide ions, must either be removed or passivated if cell efficiencies are to approach their theoretical limit. In this work, we introduce a universal double-side polymer passivation approach using ultrathin poly(methyl methacrylate) (PMMA) films. We demonstrate very high-efficiency (~20.8%) perovskite cells with some of the highest open circuit voltages (1.22 V) reported for the same 1.6 eV bandgap. Photoluminescence imaging and transient spectroscopic measurements confirm a significant reduction in non-radiative recombination in the passivated cells, consistent with the voltage increase. Analysis of the molecular interactions between

perovskite and PMMA reveals that the carbonyl (C=O) groups on the PMMA are responsible for the excellent passivation via Lewis-base electronic passivation of Pb^{2+} ions. This work provides new insights and a compelling explanation of how PMMA passivation works, and suggests future directions for developing improved passivation layers.

1. Introduction

Perovskite solar cells combine a high absorption coefficient with long carrier diffusion lengths, which are important factors explaining their rapid rise to the forefront of thin-film photovoltaics (PV).[1-6] Ever since the pioneering work by Miyasaka reporting the first perovskite solar cells with power conversion efficiencies (PCE) of ~3.8% in 2009,[7] much of the research effort has been focused on controlling the perovskite composition and morphology,[8-12] and engineering dedicated hole- and electron transport layers (HTLs and ETLs).[13-16] Combined improvements in each of these areas have led to the current PCE record of >22%.[17] Perovskite solar cell stability is also increasing, with reports of cells maintaining high-efficiency (>20%) under prolonged (~1000 hours) one-sun illumination and at elevated operating temperatures (60 ^{o}C).[18] This rapid progress is encouraging for the future commercialization of perovskite PV technology.

To date, the best-performing cells use active layers consisting of a mixed halide and mixed cation perovskite composition with a bandgap (E_g) of ~1.6 eV. The theoretical (Shockley-Queisser) PCE limit for this bandgap is >30%; well above the current experimental record.[19,20] A number of recent studies have identified non-radiative carrier recombination via defects (traps) at the perovskite-transport layer interfaces as a major source of efficiency loss in state-of-the-art cells.[19] Although the exact nature of these is still to be confirmed, both theoretical and experimental evidence points to under-coordinated Pb (Pb^{2+}) and/or halide (I^-) ions as the dominant recombination-active defects at interfaces of as-deposited films, at grain boundaries, and also in the bulk.[21-25] On a device level, non-radiative

recombination via these defects reduces the open circuit voltage (V_{oc}) and overall device performance. Interface defects have also been linked to hysteresis in current-voltage characteristics,[26,27] and may also impact long-term stability.[28] To bridge the gap between the radiative efficiency limit and experimental PCE values, it is therefore imperative to minimize the sources of recombination in perovskite films and their interfaces.[19,20]

Several recent studies suggest that interface passivation can significantly mitigate non-radiative recombination in cells, yielding both improved V_{oc} and device stability.[29-38] Many of these passivation schemes target the positively-charged Pb^{2+} defect using electron donor materials, or Lewis-bases. This general electron-passivation approach was first identified by Noel *et al.,* in Ref. [21] where perovskite films and cells treated with the Lewis bases thiophene and pyridine were shown to display significantly increased carrier lifetimes and open-circuit voltages. Since then, various other Lewis-base passivation materials have been identified, including the polymers poly(4-vinylpyridine) (PVP),[29] and PCDTBT,[30] which can be applied either as an ultrathin interface layer or blended with the perovskite precursor solution.

Other organic passivation materials include fullerenes and their derivatives (e.g. C60,[31] phenyl-C61-butyric acid methyl ester (PCBM)[32-34]), Graphene,[35] and poly(methyl methacrylate) (PMMA).[36-38] PCBM has been reported to passivate under-coordinated I atoms (I^-) at the surface and grain boundaries of perovskite films,[34] but the passivation mechanism of PMMA is not well understood. PMMA has been shown by a number of groups to effectively reduce trap density and improve cell performance when inserted as an ultrathin layer either before or after the perovskite film deposition.[36-38] This has been variously attributed to improved perovskite microstructure and surface morphology,[36,37] filling of pinholes, and unspecified passivation of surface traps.[38] PMMA has also been used as an additive during perovskite film deposition to control crystal growth and morphology, but its passivation properties in this case were not explicitly considered.[36,37]

Here, we fabricate double-side passivated perovskite cells by inserting ultrathin PMMA films at both the perovskite/ETL and perovskite/HTL interfaces. This symmetric passivating-contact structure significantly reduces interface recombination, as evidenced by improved operating voltages, and corroborated by photoluminescence (PL) imaging, time-resolved photoluminescence (TRPL), and transient absorption (TA) measurements. Double-side passivated cells have been fabricated with an efficiency of 20.8% and a remarkable V_{oc} of ~1.22 V with negligible hysteresis. This yields one of the lowest E_g - qV_{oc} values reported to date (q is the elementary charge).[39-41] The passivation mechanism is investigated using a combination of Fourier-transform infrared (FTIR) and nuclear magnetic resonance (NMR) spectroscopy measurements, supported by density functional theory (DFT) calculations. We find strong evidence that the excellent passivation provided by the PMMA films is associated with the Lewis-base nature of the oxygen atoms in the carbonyl (C=O) groups of PMMA. We thus conclude that PMMA is similar to other Lewis-base polymer passivation layers, where donor electrons can reduce the charge state of Pb^{2+} defect ions at the perovskite/ETL and perovskite/HTL interfaces, effectively reducing non-radiative recombination. This work not only demonstrates a universal, simple and effective interface passivation treatment to boost the performance of state-of-the-art perovskite solar cells, but also provides new physical insights into passivation mechanisms that could lead to further improvements in device performance.

2. Results and Discussion

To realize a perovskite solar cell with high operating voltage and negligible hysteresis, we introduce interface passivation on both the ETL and HTL sides in multi-cation perovskite cells. Our device structure is FTO/c-In-TiO_x/m-TiO_2/PMMA:PCBM/Perovskite/PMMA/Spiro-OMeTAD/Au (see **Figure 1a** and 1b), where the c-In-TiO_x,[42] m-TiO_2, Perovskite and Spiro-OMeTAD represent compact indium-doped

TiO_x, mesoporous TiO_2, $Cs_{0.07}Rb_{0.03}FA_{0.765}MA_{0.135}PbI_{2.55}Br_{0.45}$ and (2,2',7,7'-tetrakis-(N,N-di-4-methoxyphenylamino)-9,9'-spiro-bifluorene), respectively. The thickness of each layer is shown in the cross-sectional scanning electron microscope (SEM) image in Figure 1b. We use the perovskite solar cell devoid of any passivation layer as a control device, where the architecture is FTO/c-In-TiO_x/m-TiO_2/Perovskite/Spiro-OMeTAD/Au.

As seen in **Figure 2a**, the control device yielded a PCE of 19.5% from a reverse current-voltage scan, with V_{oc}= 1.110 V, short-circuit current density J_{sc} = 22.85 mA/cm^2 and fill-factor FF = 0.770. A small amount of hysteresis is also observed, with a forward scan yielding PCE=18.5%. Details of the scan rate and *J-V* measurement procedure are provided in the Supporting Information. After inserting an ultrathin PMMA:PCBM passivation layer at the m-TiO_2/perovskite interface (labeled as passivated ETL side), the V_{oc} increased to 1.170 V, yielding a PCE of ~20.3% (see Figure 2c), which is consistent with our previous work.[43] Inspired by this finding, we also inserted an ultra-thin pure PMMA film (details in the Supporting Information) at the HTL/perovskite interface. Encouragingly, this double-side passivation significantly boosted the V_{oc} to 1.213 V, resulting in a champion cell with a PCE of ~20.8% and negligible hysteresis as seen in Figure 2e. Consistent with the reduced hysteresis, we also find that the transient V_{oc} response of the double-side passivated cells is much shorter than that of the control cells, taking less than 3 s to reach their steady-state value after exposure to light (see Figure S1, Supporting Information).

Device performance was further characterized with steady-state efficiency and external quantum efficiency (EQE) measurements. Figure S2 (Supporting Information) shows the steady-state PCE of the control cell to be 18.7%, tested at its V_{mpp} (maximum power point voltage) of 0.93 V for 600 s. Notably, the steady-state PCE of the passivated cells was much improved with respect to the control device, resulting in a stabilized PCE of 20.1% (tested at V_{mpp}=0.97 V) and 20.7% (tested at V_{mpp}=1.0 V) for the ETL-side passivated cell and the double-side passivated cells, respectively. We also performed a much longer (~10 hrs) steady-

state efficiency measurement (see Figure S2d, Supporting Information), which showed that the PMMA passivation treatment effectively improves the light-soaking stability of cells. EQE measurements on the control and passivated cells show no significant variation with the addition of the passivation layers (Figure S3, Supporting Information) and the integrated current from EQE spectra are within 3% of the values obtained from current-voltage measurements.

In order to quantify more accurately the impact of the passivation layers, we fabricated and measured twenty cells for each condition (control, ETL-side passivation, double-side passivation) in two separate batches. **Figure 3** shows the detailed distribution of the performance parameters extracted from reverse-scan measurements. It is clear that the most significant impact of the passivation is to increase the V_{oc}. The average V_{oc} of the control cells is 1.10±0.01 V. This increases to 1.16±0.01 V with ETL-side passivation, and 1.20±0.01 V for the double-side passivated cells, respectively corresponding to a relative increase of 5.4% and 9.1% compared to that of control cells. At the same time, the FF and J_{sc} for the double-side passivated cells are both reduced slightly (by 2.4% and 0.5% relative, respectively), which we attribute to a small reduction in the carrier-extraction efficiency and increased series resistance resulting from the insulating PMMA film. Nevertheless, the small penalty in these parameters is more than compensated by the increased voltage. As a result, the average cell efficiency increases from 18.8±0.5% for the control cells to 19.9±0.5% for the double-side passivated cells. We also note that the best double-side passivated cell yielded a remarkable V_{oc} = 1.22 V (see also Figure S4, Supporting Information), which is amongst the highest reported values for ~1.6 eV bandgap perovskite.[39-41]

To verify that the improved device performance is a result of interface passivation, and not due to a change in bulk properties or film morphology we investigated the deposited films using X-ray diffraction (XRD) and SEM. XRD spectra reveal no systematic variations due to the passivation treatment. No obvious PbI_2 or other non-perovskite phases are observed; nor is

there a significant variation in crystallite size, as shown in Figure S5 (Supporting Information). From SEM inspection there is no significant difference in the top-morphology of perovskite films in control and passivated perovskite (see Figure S6, Supporting Information).

Subsequently, we performed PL imaging on the control and passivated cells under open-circuit conditions (see Figures 2b, 2d and 2f). The PL intensity of the best ETL-side passivated perovskite cell and double-side passivated cell increased more than 5-fold and 34-fold respectively compared to the control cell. From this, it is evident that the non-radiative recombination was significantly reduced by the PMMA:PCBM and PMMA passivation. Reduced non-radiative recombination increases the excess charge carrier density in the active layer under steady-state open circuit conditions, increasing the quasi Fermi level splitting and thus increasing the V_{oc} of the cells.[44] This further confirms the origin of the improved V_{oc} in the passivated perovskite cells. The PL images also show good passivation uniformity over the whole device area.

A reduction in recombination rate with the introduction of the PMMA layers is also observed in time-resolved PL measurements shown in **Figure 4**. Two sets of samples were prepared to investigate separately the impact of passivating the ETL and HTL interfaces. Time-resolved PL spectra were measured from the relevant transport layer side using a 650nm wavelength pulsed laser as the excitation source. The spectral evolution is shown in Figure S7 (Supporting Information); the perovskite layer shows the characteristic PL peak at 770 nm without any additional spectral feature. Figure 4a shows PL transients measured at the peak emission wavelength for representative samples with and without a passivation layer between the perovskite and the ETL (no HTL was included in these samples). To measure the impact of the extraction layer and effect of passivation on the PL dynamics, the PL transients were fitted with a sum of two exponential functions and the weighted-average lifetimes were calculated. We note that this is merely a parameterization of the PL dynamics, which lacks physical meaning. In fact, it has been shown that the photogenerated minority carrier lifetime of

perovskites is dominated by a combination of first, second, and third order recombination processes. These are respectively equivalent to trap-assisted non-radiative (Shockley-Read-Hall), band-to-band radiative (bimolecular, two-particle), and Auger (three-particle) recombination, which requires fluence-dependent experiments to separate the different processes.[45-48] However, this is beyond the scope of the present work and thus a parameterization of the decays was chosen instead. Using this parametrization of the transients, we find for the reference ETL/perovskite sample an average PL lifetime of 125 ns, whilst the one-side and two-side passivated samples exhibit longer average PL lifetimes of 195 ns and 245 ns, respectively. As reference, we also measured the pristine perovskite sample without any passivation or interface to a charge extraction layer and found a PL lifetime of 738 ns. The PL average lifetime quenching observed upon addition of the ETL is attributed to a combined effect of carrier extraction (by the ETL) and interface recombination.[25,49] The significant lifetime recovery observed with the addition of the ultrathin PMMA passivation layer indicates reduced interface recombination and efficient passivation of trap states and recombination centers.

Figure 4b shows PL transients for perovskite/HTL samples with and without the PMMA passivation layer (without using ETL in this configuration). Interestingly, the average PL lifetime is comparably shorter than for the ETL/perovskite samples, specifically 27 ns for the perovskite/HTL sample compared to 125 ns for the ETL/perovskite and 738 ns for the neat perovskite film, implying very fast extraction and / or introduction of significant surface recombination. However, inserting a PMMA passivation layer at the perovskite/HTL interface results in a significant increase in the PL lifetime from 27 ns to 70 ns.

Recombination dynamics were also investigated with transient absorption (TA) spectroscopy in the nano-to-microsecond time window using a 532 nm pulsed laser excitation source (see Supporting Information for details). Similar to the transient PL measurements, separate samples were prepared to study the ETL/perovskite and perovskite/HTL interfaces with and

without a passivation layer. TA measurements were performed with the pump and probe light incident from the side closest to the interface of interest. As with the PL measurements, adding charge extraction layers leads to faster dynamics compared to neat perovskite films, while the passivated samples exhibited slower decay dynamics compared to the non-passivated samples (see Figure S8, Supporting Information).

The results presented so far show that inserting ultrathin PMMA films at the ETL/perovskite and HTL/perovskite interfaces can dramatically increase the open-circuit voltage of our cells without significant impact on the short-circuit current or fill-factor. This is accompanied by both increased PL intensity and increased carrier lifetime in the perovskite active layer, indicating a strong reduction in non-radiative carrier recombination. We thus conclude that the PMMA films can effectively passivate interface traps/defects on both sides of the perovskite active layer while still allowing efficient carrier extraction into the charge transport layers.

We next investigate the physical origin of the passivation mechanism and the nature of the interface traps/defects being passivated. To do this, we use Fourier transform infrared (FTIR) and nuclear magnetic resonance (NMR) spectroscopy, combined with numerical simulations to identify the molecular-level interactions at the perovskite-PMMA interface.

In a previous study of polymer-templated perovskite films, Bi *et al*.[36] used FTIR to study films of PMMA and PMMA + PbI_2. The spectral feature associated with the stretching vibration of the C=O covalent bond in the PMMA was found to red-shift with the addition of the Lewis acid PbI_2. This was attributed to the formation of an intermediate PMMA-PbI_2 adduct that influenced film crystallization. In a related study, Masi *et al*.[37] proposed electrostatic interactions between the same C=O (carbonyl) group and positively-charged MA^+ precursor ions as playing a key role in film morphology.

Here we first use FTIR to probe the stretching vibration of the C=O bond in thin films of pure PMMA, PMMA + PbI_2, PMMA + PbI_2 + $PbBr_2$, and PMMA + formamidinium iodide (FAI).

As can be seen in **Figure 5a**, the C=O spectral feature associated with this bond in pure PMMA film appears at 1732 cm^{-1}, but shifts to 1724 cm^{-1} and 1725 cm^{-1} with the addition of PbI_2 and mixed PbI_2 + $PbBr_2$, respectively. This indicates a weakening of the C=O bond similar to the results of Bi *et al.*[36] Interestingly, a larger spectral shift (to 1720 cm^{-1}) is measured for the PMMA + FAI thin film, which is consistent with the electrostatic interaction proposed by Masi *et al.*, but involving FA^+ ions rather than MA^+. To confirm that the dominant interaction between PMMA and perovskite is via the C=O group (and not one of the other functional groups), we also measured 1H NMR spectra of PMMA, PMMA + PbI_2 and PMMA + FAI in DMSO-d6 solution. Figure 5b shows that excess PbI_2 or FAI does not affect the chemical shift of protons on PMMA, indicating that there is no significant interaction between PbI_2 or FAI with the saturated C atom or H atom on the PMMA chain. Thus, we have strong evidence that the PMMA carbonyl group can interact with multiple perovskite precursor species, the most likely in this case being positively charged Pb^{2+} and FA^+ ions.

The oxygen atom in a carbonyl group is a Lewis base (electron donor) site due to the electron pair associated with the C=O double bond.[50] This is clearly observed as local negative electrical charge (blue) surrounding the oxygen atoms in Figure 5c, which plots the electrostatic potential of a PMMA chain calculated using Density Functional Theory (DFT). The interaction between this local negative charge and the Pb^{2+} and FA^+ ions explains the red-shift observed in the FTIR spectra (Figure 5a). The role of Pb^{2+} defects as recombination centers on the surface and grain boundaries of solid perovskite films is widely accepted, as is the ability of Lewis base materials to passivate these defects.[21] Therefore we conclude that the improved carrier lifetime and higher photoluminescence of films and cells shown in Figures 2 and 4 are a direct consequence of PMMA passivating under-coordinated Pb atoms at the perovskite/ETL and perovskite/HTL interfaces. This leads to the outstanding open circuit voltages and improved cell efficiencies of double-side passivated cells demonstrated in Figure 2.

To further confirm the universality of our double-side passivation approach, we tested two more sets of different types of perovskite solar cells using PMMA passivation layers. As demonstrated in the **Figure 6a**, all cells with double-side passivation exhibit much higher V_{oc} than the corresponding non-passivated (control) cells, boosting their performance. The double-side passivation also significantly suppressed the *J-V* hysteresis behaviour of all cells (see Figure 6b). The detailed *J-V* curves and *J-V* parameters are also provided in Figure S9 and Table S1 (Supporting Information).

3. Conclusion

In summary, we demonstrated a universal double-side passivation method that passivates perovskite solar cells incorporating ultrathin PMMA-films at the perovskite-ETL and perovskite-HTL interfaces. The outstanding passivation properties of the PMMA enabled open circuit voltages up to ~1.22 V, which is one of the highest reported for ~1.6 eV bandgap perovskite. A high PCE of 20.8% with negligible hysteresis was achieved for the champion passivated cells. Analysis of perovskite-PMMA interactions reveals that the passivation results from the Lewis-base properties of the carbonyl (C=O) group on the PMMA, which can effectively passivate under-coordinated lead atoms (Pb^{2+}), which are thought to cause non-radiative recombination at perovskite surfaces and grain boundaries. This finding sheds new light on previous work involving PMMA passivation layers, and may provide additional explanation for the improved performance of PMMA-templated perovskite films.[36,37]

Although it provides excellent interface passivation, PMMA is an insulating polymer so the passivated cells did have a slightly reduced fill-factor as a result of increased series resistance. This was mitigated on the ETL side by using a PMMA:PCBM blend, as reported previously,[43] but future development of novel conducting polymers with C=O groups may lead to even further efficiency gains.

Experimental Section
Experimental details are provided in Supporting Information.

Supporting Information
Supporting Information is available from the Wiley Online Library or from the author.

Acknowledgements
This work was supported by the Australian Government through the Australian Renewable Energy Agency (ARENA) and the Australian Research Council. Responsibility for the views, information or advice expressed herein is not accepted by the Australian Government. J. P. acknowledges the funding support from Australian Nanotechnology Network (ANN) and Department of Innovation, Industry, Science and Research (DIISR). The research reported in this publication was supported by funding from King Abdullah University of Science and Technology (KAUST). Authors thank Xavier Pita, scientific illustrator at King Abdullah University of Science and Technology (KAUST), for producing the Figure 1A in this paper.

Author Contributions
J. P. conceived the idea, designed the overall experiments and led the project. J. P., T. D., H. S. and Y. W. prepared and characterized the perovskite cell devices. J. I. K. and E. U. performed the TA and TRPL measurements and data analysis. F. L. supervised the TA and TRPL measurements and analysis. W. L., X. Y. and J. P. conducted the FTIR measurements and analysis. W. L. performed the DFT calculation. T. D., H. S. and Y. W. conducted the PL imaging measurements. H. D. conducted the XRD and SEM measurements. K. W. conducted the NMR measurements and analysis. E. A. conducted the EQE measurements. J. P., J. I. K., K. J. W., K. R. C., F. L., S. D. W. and T. P. W. contributed to the results analysis and interpretation. T. P. W. and S. D. W. supervised the project. J. P. wrote the manuscript. All authors contributed to the discussion of the results and revision of the manuscript.

Received: ((will be filled in by the editorial staff))
Revised: ((will be filled in by the editorial staff))
Published online: ((will be filled in by the editorial staff))

References

[1] S. D. Stranks, G. E. Eperon, G. Grancini, C. Menelaou, M. J. Alcocer, T. Leijtens, L. M. Herz, A. Petrozza and H. J. Snaith, *Science* **2013**, *342*, 341.
[2] G. Xing, N. Mathews, S. Sun, S. S. Lim, Y. M. Lam, M. Grätzel, S. Mhaisalkar and T. C. Sum, *Science* **2013**, *342*, 344.
[3] M. M. Lee, J. Teuscher, T. Miyasaka, T. N. Murakami and H. J. Snaith, *Science* **2012**, *338*, 643.
[4] W. Nie, H. Tsai, R. Asadpour, J.-C. Blancon, A. J. Neukirch, G. Gupta, J. J. Crochet, M. Chhowalla, S. Tretiak, M. A. Alam, H.-L. Wang and A. D. Mohite, *Science* **2015**, *347*, 522.
[5] H. Zhou, Q. Chen, G. Li, S. Luo, T.-B. Song, H.-S. Duan, Z. Hong, J. You, Y. Liu and Y. Yang, *Science* **2014**, *345*, 542.

[6] V. D'Innocenzo, G. Grancini, M. J. Alcocer, A. R. S. Kandada, S. D. Stranks, M. M. Lee, G. Lanzani, H. J. Snaith and A. Petrozza, *Nat. Commun.* **2014**, *5*, 3586.
[7] A. Kojima, K. Teshima, Y. Shirai and T. Miyasaka, *J. Am. Chem. Soc.* **2009**, *131*, 6050.
[8] J. Burschka, N. Pellet, S.-J. Moon, R. Humphry-Baker, P. Gao, M. K. Nazeeruddin and M. Grätzel, *Nature* **2013**, *499*, 316.
[9] J. W. Lee, D. J. Seol, A. N. Cho and N. G. Park, *Adv. Mater.* **2014**, *26*, 4991.
[10] N. J. Jeon, J. H. Noh, W. S. Yang, Y. C. Kim, S. Ryu, J. Seo and S. I. Seok, *Nature* **2015**, *517*, 476.
[11] Z. Wang, Q. Lin, F. P. Chmiel, N. Sakai, L. M. Herz and H. J. Snaith, *Nat. Energy* **2017**, *2*, 17135.
[12] A. D. Jodlowski, C. Roldán-Carmona, G. Grancini, M. Salado, M. Ralaiarisoa, S. Ahmad, N. Koch, L. Camacho, G. De Miguel and M. K. Nazeeruddin, *Nat. Energy* **2017**, *2*, 972.
[13] J. A. Christians, P. Schulz, J. S. Tinkham, T. H. Schloemer, S. P. Harvey, B. J. T. de Villers, A. Sellinger, J. J. Berry and J. M. Luther, *Nat. Energy* **2018**, *3*, 68.
[14] M. Li, Z. K. Wang, Y. G. Yang, Y. Hu, S. L. Feng, J. M. Wang, X. Y. Gao and L. S. Liao, *Adv. Energy Mater.* **2016**, *6*, 1601156.
[15] W. Chen, Y. Wu, Y. Yue, J. Liu, W. Zhang, X. Yang, H. Chen, E. Bi, I. Ashraful and M. Grätzel, *Science* **2015**, *350*, 944.
[16] Y. Hou, X. Du, S. Scheiner, D. P. McMeekin, Z. Wang, N. Li, M. S. Killian, H. Chen, M. Richter, I. Levchuk, N. Schrenker, E. Spiecker, T. Stubhan, N. A. Luechinger, A. Hirsch, P. Schmuki, H.-P. Steinruck, R. H. Fink, M. Halik, H. J. Snaith and C. J. Brabec, *Science* **2017**, *358*, 1192.
[17] W. S. Yang, B. W. Park, E. H. Jung, N. J. Jeon, Y. C. Kim, D. U. Lee, S. S. Shin, J. Seo, E. K. Kim, J. H. Noh and S. II. Seok, *Science* **2017**, *356*, 1376.
[18] N. Arora, M. I. Dar, A. Hinderhofer, N. Pellet, F. Schreiber, S. M. Zakeeruddin and M. Grätzel, *Science* **2017**, DOI: 10.1126/science.aam5655.
[19] [a)] P. Schulz, *ACS Energy Lett.* **2018**, *3*, 1287; [b)] S. D. Stranks, *ACS Energy Lett.* **2017**, *2*, 1515; [c)] J. -P. Correa-Baena, W. Tress, K. Domanski, E. H. Anaraki, S. -H. Turren-Cruz, B. Roose, P. P. Boix, M. Grätzel, M. Saliba, A. Abate and A. Hagfeldt, *Energy Environ. Sci.* **2017**, *10*, 1207; [d)] K. K. Wong, A. Fakharuddin, P. Ehrenreich, T. Deckert, M. Abdi-Jalebi, R. H. Friend and L. Schmidt-Mende, *J. Phys. Chem. C* **2018**, *122*, 10691; [e)] M. Stolterfoht, C. M. Wolff, J. A. Marquez, S. Zhang, C. J. Hages, D. Rothhardt, S. Albrecht, P. L. Burn, P. Meredith, T. Unold and D. Neher, *Nat. Energy* **2018**, DOI: 10.1038/s41560-018-0219-8.
[20] W. Tress, *Adv. Energy Mater.* **2017**, *7*, 1602358.
[21] N. K. Noel, A. Abate, S. D. Stranks, E. S. Parrott, V. M. Burlakov, A. Goriely and H. J. Snaith, *ACS Nano* **2014**, *8*, 9815.
[22] I. A. Shkrob and T. W. Marin, *J. Phys. Chem. Lett.* **2014**, *5*, 1066.
[23] W.-J. Yin, T. Shi and Y. Yan, *Appl. Phys. Lett.* **2014**, *104*, 063903.
[24] [a)] Z. Xiao, Y. Yuan, Y. Shao, Q. Wang, Q. Dong, C. Bi, P. Sharma, A. Gruverman and J. Huang, *Nat. Mater.* **2015**, *14*, 193; [b)] H. Uratani and K. Yamashita, *J. Phys. Chem. Lett.* **2017**, *8*, 742.
[25] A. Abate, M. Saliba, D. J. Hollman, S. D. Stranks, K. Wojciechowski, R. Avolio, G. Grancini, A. Petrozza and H. J. Snaith, *Nano Lett.* **2014**, *14*, 3247.
[26] B. Chen, M. Yang, S. Priya and K. Zhu, *J. Phys. Chem. Lett.* **2016**, *7*, 905-917.
[27] W. Tress, N. Marinova, T. Moehl, S. M. Zakeeruddin, M. K. Nazeeruddin and M. Grätzel, *Energy Environ. Sci.* **2015**, *8*, 995.
[28] F. Huang, L. Jiang, A. R. Pascoe, Y. Yan, U. Bach, L. Spiccia and Y.-B. Cheng, *Nano Energy* **2016**, *27*, 509.

[29] [a] B. Chaudhary, A. Kulkarni, A. K. Jena, M. Ikegami, Y. Udagawa, H. Kunugita, K. Ema and T. Miyasaka, *ChemSusChem* **2017**, *10*, 2473; [b] L. Zuo, H. Guo, S. Jariwala, N. De Marco, S. Dong, R. DeBlock, D. S. Ginger, B. Dunn, M. Wang and Y. Yang, *Sci. Adv.* **2017**, *3*, e1700106.
[30] C.-C. Zhang, M. Li, Z.-K. Wang, Y.-R. Jiang, H.-R. Liu, Y.-G. Yang, X.-Y. Gao and H. Ma, *J. Mater. Chem. A* **2017**, *5*, 2572.
[31] H. Yoon, S. M. Kang, J.-K. Lee and M. Choi, *Energy Environ. Sci.* **2016**, *9*, 2262.
[32] Y. Shao, Z. Xiao, C. Bi, Y. Yuan and J. Huang, *Nat. Commun.* **2014**, *5*, 5784.
[33] C. Tao, S. Neutzner, L. Colella, S. Marras, A. R. S. Kandada, M. Gandini, M. De Bastiani, G. Pace, L. Manna, M. Caironi, C. Nertarelli and A. Petrozza, *Energy Environ.Sci.* **2015**, *8*, 2365.
[34] Y. Zhao, W. Zhou, W. Ma, S. Meng, H. Li, J. Wei, R. Fu, K. Liu, D. Yu and Q. Zhao, *ACS Energy Lett.* **2016**, *1*, 266.
[35] A. Agresti, S. Pescetelli, B. Taheri, A. E. Del Rio Castillo, L. Cina, F. Bonaccorso and A. Di Carlo, *ChemSusChem.* **2016**, *9*, 2609.
[36] D. Bi, C. Yi, J. Luo, J.-D. Décoppet, F. Zhang, S. M. Zakeeruddin, X. Li, A. Hagfeldt and M. Grätzel, *Nat. Energy* **2016**, *1*, 16142.
[37] S. Masi, A. Rizzo, F. Aiello, F. Balzano, G. Uccello-Barretta, A. Listorti, G. Gigli and S. Colella, *Nanoscale* **2015**, *7*, 18956.
[38] F. Wang, A. Shimazaki, F. Yang, K. Kanahashi, K. Matsuki, Y. Miyauchi, T. Takenobu, A. Wakamiya, Y. Murata and K. Matsuda, *J. Phys. Chem. C* **2017**, *121*, 1562.
[39] H. Tan, A. Jain, O. Voznyy, X. Lan, F. P. G. de Arquer, J. Z. Fan, R. Quintero-Bermudez, M. Yuan, B. Zhang and Y. Zhao, F. Fan, P. Li, L. Quan, Y. Zhao, Z.-H. Lu, Z. Yang, S. Hoogland and E. H. Sargent, *Science*, **2017**, *355*, 722.
[40] M. Saliba, T. Matsui, K. Domanski, J.-Y. Seo, A. Ummadisingu, S. M. Zakeeruddin, J.-P. Correa-Baena, W. R. Tress, A. Abate, A. Hagfeldt and M. Gratzel, *Science* **2016**, *354*, 206.
[41] E. H. Anaraki, A. Kermanpur, L. Steier, K. Domanski, T. Matsui, W. Tress, M. Saliba, A. Abate, A. Abate, M. Grätzel, A. Hagfeldt and J.-P. Correa-Baena, *Energy Environ. Sci.* **2016**, *9*, 3128.
[42] J. Peng, T. Duong, X. Zhou, H. Shen, Y. Wu, H. K. Mulmudi, Y. Wan, D. Zhong, J. Li, T. Tsuzuki, K. J. Weber, K. R. Catchpole and T. P. White, *Adv. Energy Mater.* **2017**, *7*, 1601768.
[43] J. Peng, Y. Wu, W. Ye, D. A. Jacobs, H. Shen, X. Fu, Y. Wan, T. Duong, N. Wu, C. Barugkin and H. T. Nguyen, D. Zhong, J. Li, T. Lu, Y. Liu, M. N. Lockrey, K. J . Weber, K. R. Catchpole and T. P. White, *Energy Environ. Sci.* **2017**, *10*, 1792.
[44] M. I. Dar, M. Franckevičius, N. Arora, K. Redeckas, M. Vengris, V. Gulbinas, S. M. Zakeeruddin and M. Grätzel, *Chem. Phys. Lett.* **2017**, *683*, 211.
[45] J. M. Richter, M. Abdi-Jalebi, A. Sadhanala, M. Tabachnyk, J. P. Rivett, L. M. Pazos-Outón, K. C. Gödel, M. Price, F. Deschler and R. H. Friend, *Nat. Commun.* **2016**, *7*, 13941.
[46] J. M. Ball and A. Petrozza, *Nat. Energy* **2016**, *1*, 16149.
[47] L. M. Herz, Annu. *Rev. Phys. Chem.* **2016**, *67*, 65.
[48] C. L. Davies, M. R. Filip, J. B. Patel, T. W. Crothers, C. Verdi, A. D. Wright, R. L. Milot, F. Giustino, M. B. Johnston and L. M. Herz, *Nat. Commun.* **2018**, *9*, 293.
[49] Y. Yang, M. Yang, D. T. Moore, Y. Yan, E. M. Miller, K. Zhu and M. C. Beard, *Nat. Energy* **2017**, *2*, 16207.
[50] A. T. Hubbard, Encyclopaedia of Surface and Colloid Science P.77, Vol. 1 (New York: Marcel Dekker, 2002).

[51] T. Duong, Y. Wu, H. Shen, J. Peng, X. Fu, D. Jacobs, E-C. Wang, T. C. Kho, K. C. Fong, M. Stocks, E. Franklin, A. Blakers, N. Zin, K. Mclntosh, W. Li, Y.-B. Cheng, T. P. White, K. Weber and K. Catchpole, *Adv. Energy Mater.* **2017**, *7*, 1700228.

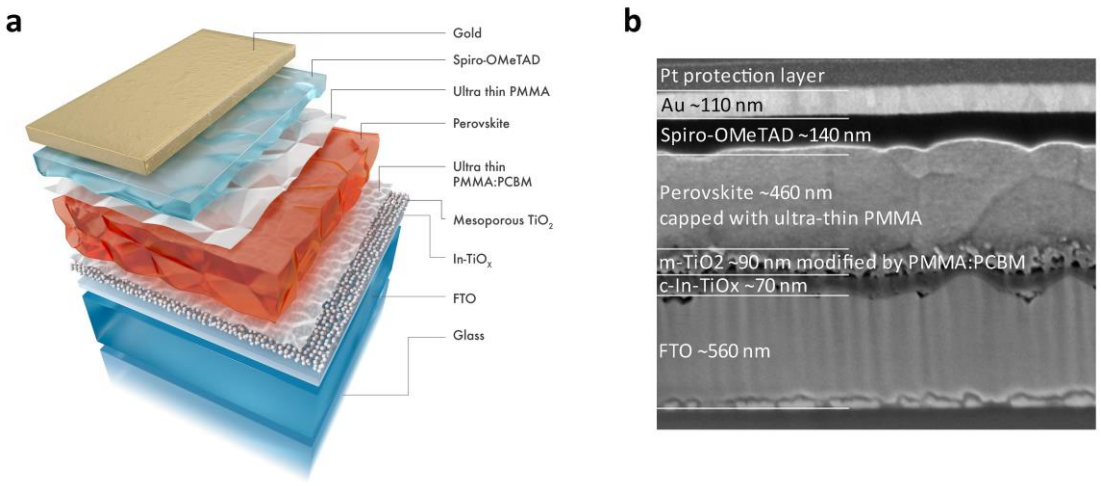

Figure 1. Schematic of the device structure and corresponding SEM cross-sectional image. a) Schematic of the device structure. b) SEM cross-sectional image of the perovskite cell. Note that the Pt protection layer seen in (b) was only used to prepare the focused ion beam (FIB) SEM cross-sectional image. 'Perovskite' refers here to the composition $Cs_{0.07}Rb_{0.03}FA_{0.765}MA_{0.135}PbI_{2.55}Br_{0.45}$.

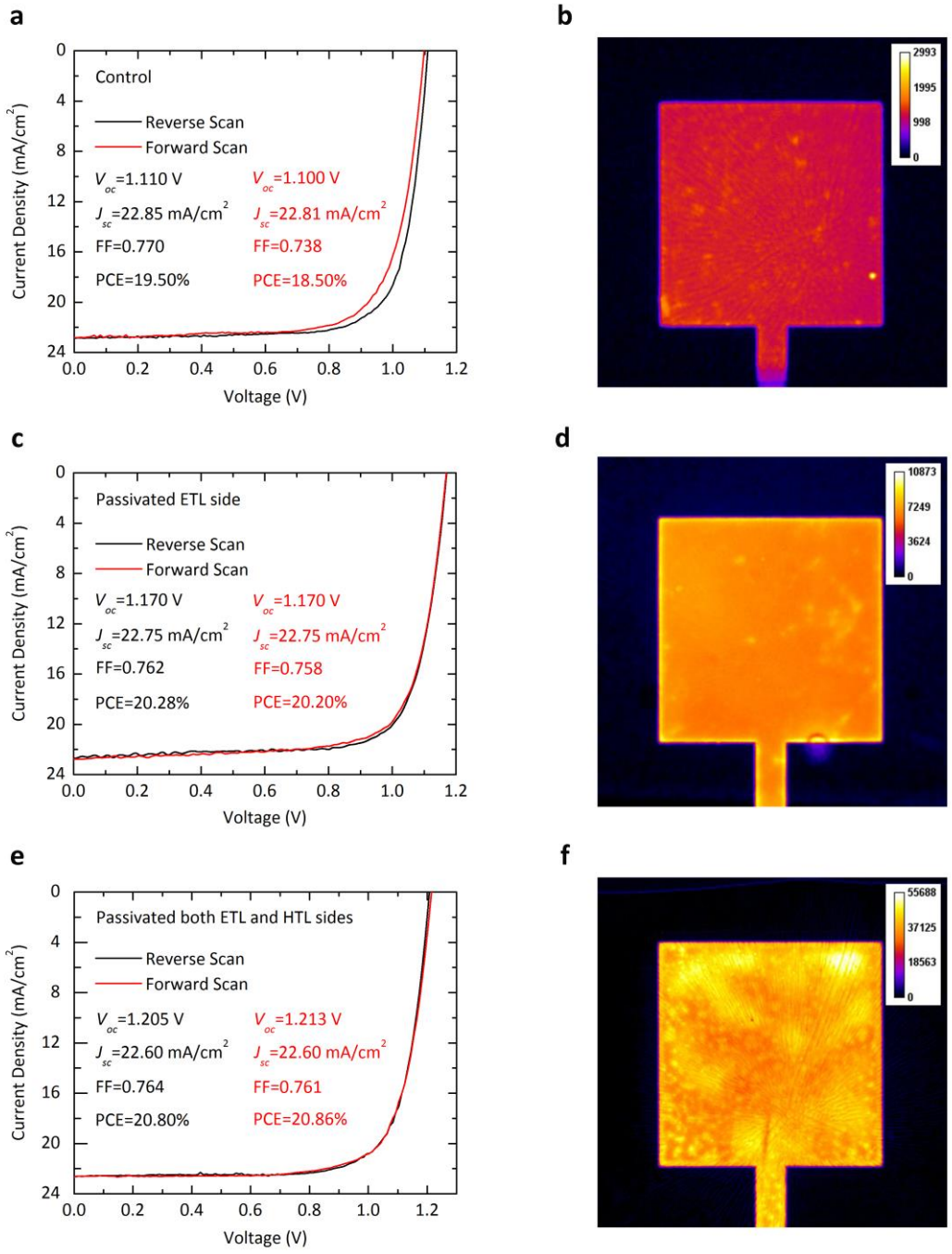

Figure 2. Device performance and PL imaging. a) and b) Forward- and reverse-scan *J-V* curves of the control cell with a structure of FTO/c-In-TiO_x/m-TiO_2/Perovskite/Spiro-OMeTAD/Au, and its corresponding photoluminescence (PL) image. c) and d) *J-V* curves of the passivated ETL side cell with a structure of FTO/c-In-TiO_x/m-TiO_2/PMMA:PCBM/Perovskite/Spiro-OMeTAD/Au, and its corresponding PL image. e) and f) *J-V* curves of the double-side passivated cell with a structure of FTO/c-In-TiO_x/m-TiO_2/PMMA:PCBM/Perovskite/PMMA/Spiro-OMeTAD/Au, and its corresponding PL image. 'Perovskite' refers to the composition $Cs_{0.07}Rb_{0.03}FA_{0.765}MA_{0.135}PbI_{2.55}Br_{0.45}$.

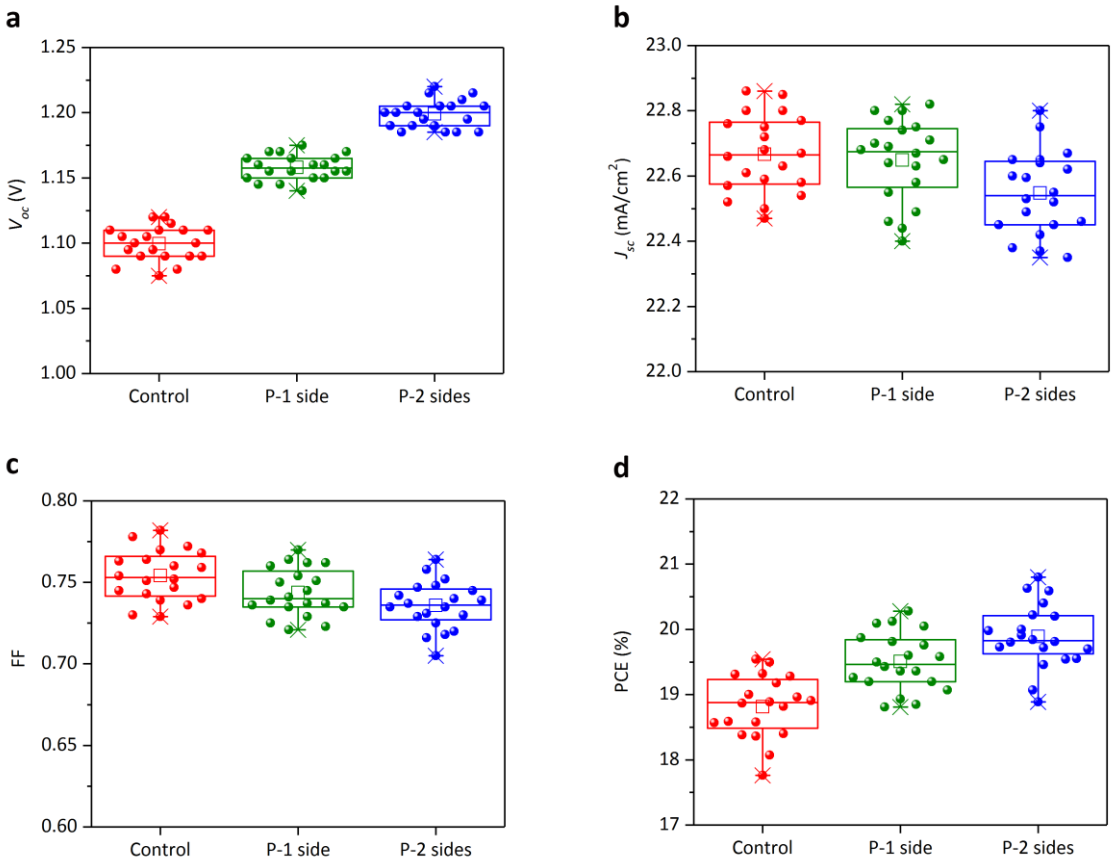

Figure 3. Statistical distribution of the photovoltaic parameters for control and passivated cells with/without PMMA:PCBM and PMMA passivation layer. a) Distribution of V_{oc}. b) Distribution of J_{sc}. c) Distribution of FF. d) Distribution of PCE. Note that 'control' represents the control cells with a structure of FTO/c-In-TiO_x/m-TiO_2/Perovskite/Spiro-OMeTAD/Au; 'P-1 side' represents the passivated ETL side cells with a structure of FTO/c-In-TiO_x/m-TiO_2/PMMA:PCBM/Perovskite/Spiro-OMeTAD/Au; the 'P-2 side' represents the double-side passivated cells with a structure of FTO/c-In-TiO_x/m-TiO_2/PMMA:PCBM/Perovskite/PMMA/Spiro-OMeTAD/Au. 'Perovskite' represents $Cs_{0.07}Rb_{0.03}FA_{0.765}MA_{0.135}PbI_{2.55}Br_{0.45}$. Results are shown for 60 cells (20 cells for each condition) collected from 2 different batches. All devices were tested at a 50 mV s^{-1} reverse scan rate.

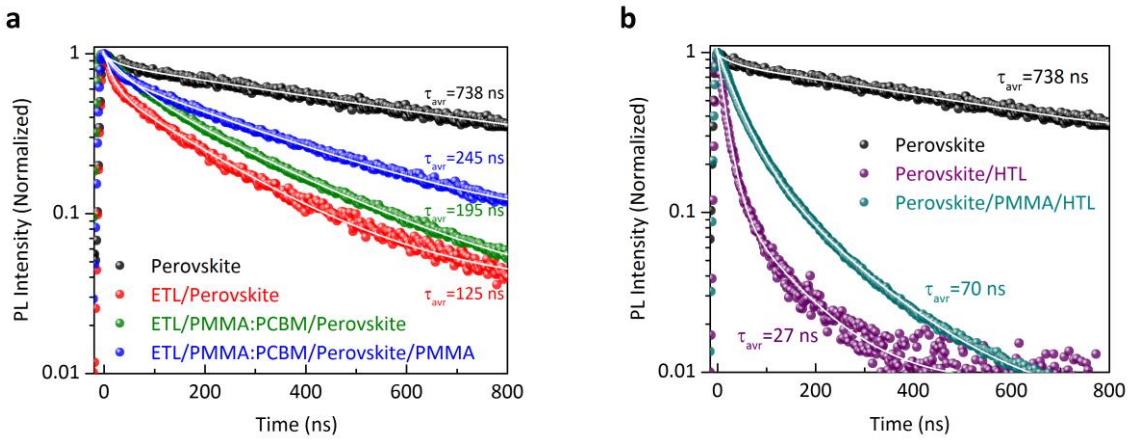

Figure 4. Photoluminescence dynamics from time-resolved (TR-PL) measurements. a) ETL only samples (illuminated from the ETL side): perovskite, ETL/perovskite, ETL/PMMA:PCBM/Perovskite and ETL/PMMA:PCBM/Perovskite/PMMA. b) HTL only samples (illuminated from the HTL side): perovskite, perovsite/HTL and perovskite/PMMA/HTL. Note that all samples were fabricated on high-grade optical quartz substrates. ETL, HTL and perovskite represent c-In-TiO_x/m-TiO_2, Spiro-OMeTAD and $Cs_{0.07}Rb_{0.03}FA_{0.765}MA_{0.135}PbI_{2.55}Br_{0.45}$, respectively.

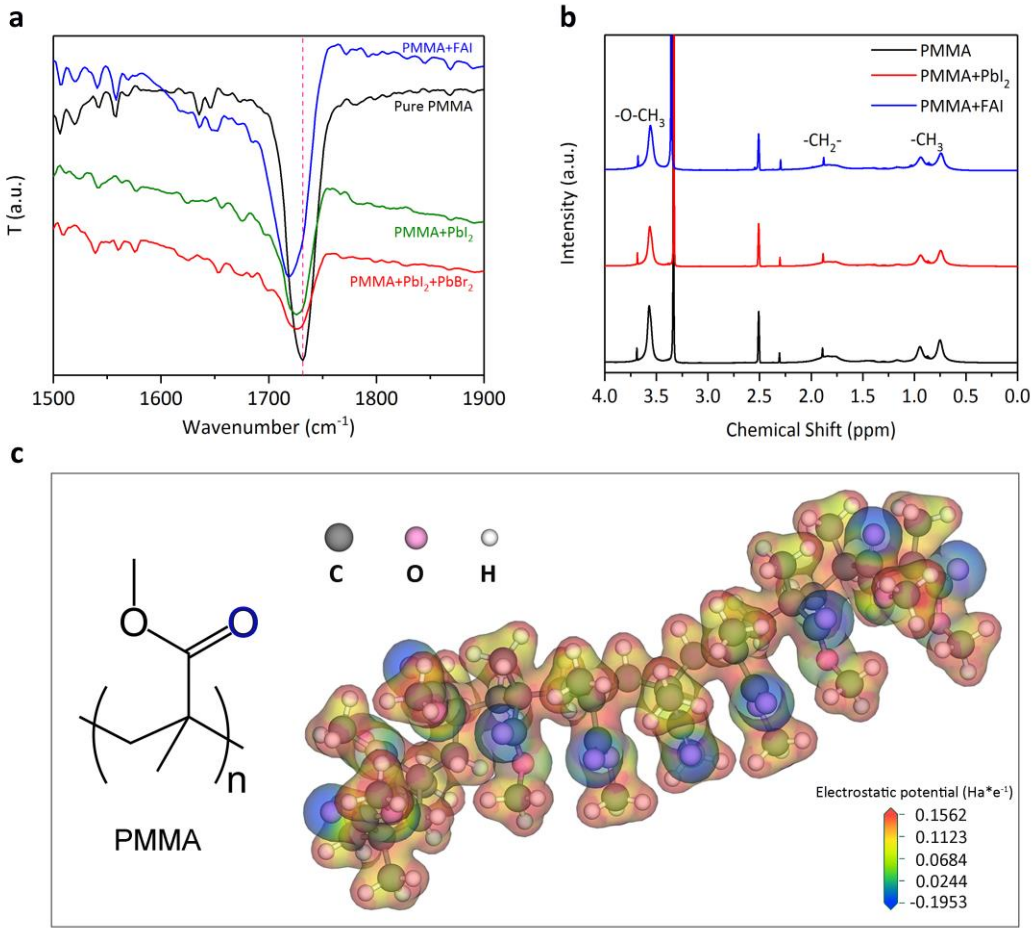

Figure 5. FTIR, NMR measurements and DFT calculation. a) FTIR spectra of pure PMMA, PMMA + PbI_2, PMMA + PbI_2 + $PbBr_2$ and PMMA + FAI thin film samples. b) 1H NMR spectra of pure PMMA, PMMA + PbI_2 and PMMA + FAI. c) Schematic diagram of the first-principle DFT calculation of the electrostatic potential for all functional groups on the PMMA chain. Details of the sample preparation are provided in the Supproting Information.

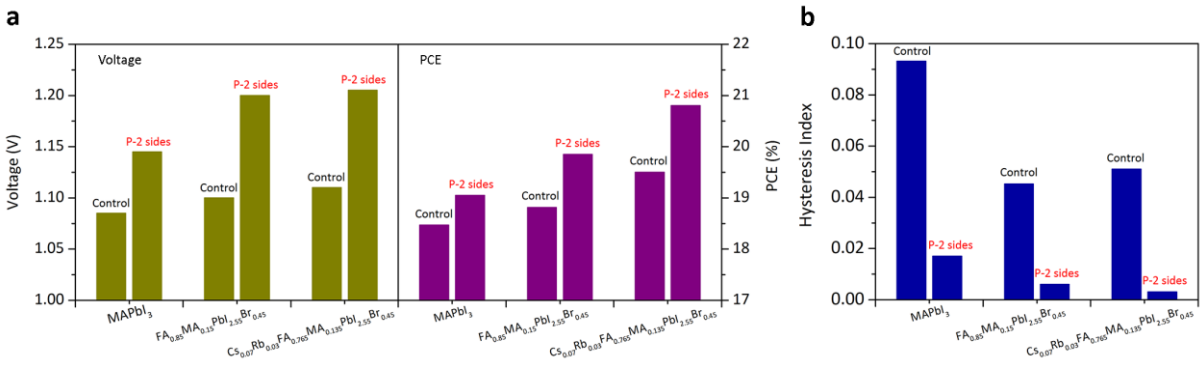

Figure 6. a) V_{oc} and PCE distribution of perovskite solar cells with different perovskite compositions. b) Hysteresis index comparison of perovskite solar cells with and without passivation. Note that 'P-2 sides' represents double-side passivation; and all devices were tested at a scan rate of 50 mV/s. The hysteresis index is defined as: $|(PCE_{reverse} - PCE_{forward})|/ PCE_{reverse}$.[51]

Interface recombination is a dominant loss mechanism in perovskite solar cells. Double-side passivation of perovskite solar cells using ultrathin films of poly(methyl methacrylate) (PMMA) can boost open circuit voltages up to 1.22 V. This results from the carbonyl (C=O) group of the Lewis-base polymer PMMA, which effectively passivates under-coordinated Pb atoms (Pb^{2+}) at the perovskite/transport layer interfaces.

Keyword

non-radiative recombination, under-coordinated Pb atoms, passivation, carbonyl group, perovskite solar cells

Jun Peng, Jafar I. Khan, Wenzhu Liu, Esma Ugur, The Duong, Yiliang Wu, Heping Shen, Kai Wang, Hoang Dang, Erkan Aydin, Xinbo Yang, Yimao Wan, Klaus J. Weber, Kylie R. Catchpole, Frédéric Laquai, Stefaan De Wolf*, Thomas P. White*

Title: A Universal Double-Side Passivation for High Open-Circuit Voltage in Perovskite Solar Cells: Role of Carbonyl Groups in Poly(methyl methacrylate)